

# Magma mingling as indicated by texture and Sr/Ba ratios of plagioclase phenocrysts from Unzen volcano, SW Japan

Brandon L. Browne<sup>a,\*</sup>, John C. Eichelberger<sup>a</sup>, Lina C. Patino<sup>b</sup>, Thomas A. Vogel<sup>b</sup>,  
Kozo Uto<sup>c</sup>, Hideo Hoshizumi<sup>c</sup>

<sup>a</sup> University of Alaska Fairbanks Geophysical Institute, Fairbanks, AK 99775, USA

<sup>b</sup> Michigan State University, Department of Geological Sciences, East Lansing, MI 48824, USA

<sup>c</sup> Geological Survey of Japan, Higashi 1-1-3, Tsukuba, 305-8567, Japan

Received 14 July 2004; accepted 30 September 2005

Available online 17 February 2006

## Abstract

Textural and geochemical characteristics of plagioclase phenocrysts from the eruptive products of Mount Unzen (SW Japan) record repeated intrusions of basaltic magma into a dacitic host magma chamber over the lifetime of the volcano. An important aspect of this mixing style is the exchange of phenocrysts between the intruding basaltic magma and host dacite magma, and the effect that this wide-reaching mixing style has on the mineralogical diversity of the erupted products. Plagioclase phenocrysts that originally crystallized from the host dacite magma are identified by oscillatory zoning patterns, low An content cores (An<sub>45</sub> to An<sub>60</sub>), and low Sr/Ba ratios. Host-derived plagioclase phenocrysts are engulfed during intrusion of basaltic magma, evidenced by their presence in basaltic to andesitic enclaves. In response to changes in temperature and composition of the surrounding melt, the engulfed plagioclases develop resorption zones, which are composed of a densely packed network of micron-sized glass inclusions and high An content plagioclase (An<sub>72</sub>–An<sub>92</sub>) with high Sr/Ba ratios that match those of plagioclase microphenocrysts inherent to the enclave-forming magma. Over time, host-derived plagioclase phenocrysts that were once engulfed during replenishment events are recycled back to the host as enclaves disaggregate (e.g. [Clynne, M.A., 1989. The disaggregation of quenched magmatic inclusions contributes to chemical diversity in silicic lavas of Lassen Peak, California. Bull New Mexico Bureau of Mines and Mineral Resources, 131: 54]). An eruption of andesite lava with no enclaves, something particularly unique for Unzen, occurred in 1663. Similar to enclaves, all plagioclase phenocrysts in this lava flow are surrounded by resorption zones suggesting that the 1663 lava may represent a magma that was erupted after thoroughly mixing with the intruding basaltic. Using experimentally calibrated crystallization rates, we estimate that phenocrysts exist in the Unzen chamber a minimum of 0.5–3 months between the time of their encounter with a basaltic intrusion and eruption.

© 2006 Elsevier B.V. All rights reserved.

**Keywords:** magma mixing; plagioclase; trace elements; enclaves; Unzen volcano; laser ablation ICP-MS

## 1. Introduction

The bulk composition of many intermediate volcanic rocks typically represent a combination of processes such as magma mixing, fractional crystallization, and contamination that modify magmas after they separate

\* Corresponding author. Current Contact Information: Department of Geological Sciences, California State University, Fullerton, Fullerton CA 92834, USA. Tel.: +1 714 278 3054.

E-mail address: [bbrowne@fullerton.edu](mailto:bbrowne@fullerton.edu) (B.L. Browne).

from their source. This makes interpretation of whole-rock data difficult. In order to achieve a more comprehensive understanding of these processes, petrologic studies commonly utilize a combination of whole-rock and mineral compositional data, and textural characteristics of individual phenocrysts. Textural characteristics of phenocrysts are often used to infer magmatic process (Tsuchiyama and Takahashi, 1983; Nelson and Montana, 1992; Nakada et al., 1994; Dunbar et al., 1994; Singer et al., 1995; Feeley and Dungan, 1996; Izbekov et al., 2002). Isotopic compositions of phenocrysts have been used to great advantage in studying processes such as magma mixing and contamination, since they may be considered as a kind of “petrological fingerprint” (Davidson and Tepley, 1997; Davidson et al., 1998; Knesel et al., 1999; Tepley et al., 1999, 2000; Davidson et al., 2001). Major and trace element compositions of individual phenocrysts have also been employed in similar ways to investigate contamination and mixing (Singer et al., 1995; Bindeman and Bailey, 1999; Izbekov et al., 2002). Geochemical results from studies such as these conclude that many crystals did not grow from the magma in which they are hosted during eruption.

Chemical and textural zoning patterns preserved in plagioclase phenocrysts provide useful information that constrains changing melt-crystal compositions, and therefore bear on the general problem of how magmas of differing compositions and physical properties chemically interact in shallow reservoirs beneath arc volcanoes. Many studies have utilized the compositional and textural information recorded in plagioclase from volcanic rocks to infer various aspects of magma chamber dynamics (Lofgren, 1980; Heiken and Eichelberger, 1980; Anderson, 1983; Tsuchiyama and Takahashi, 1983; Pearce et al., 1987; Geist et al., 1988; Druitt and Bacon, 1989; Stimac et al., 1990; Nelson and Montana, 1992; Stimac and Pearce, 1992; Singer et al., 1995; Feeley and Dungan, 1996; Pallister et al., 1996; Davidson and Tepley, 1997; Nakamura and Shimakita, 1998; Davidson et al., 1998; Clynne, 1999; Gamble et al., 1999; Tepley et al., 1999; Zellmer et al., 1999; Tepley et al., 2000; Davidson et al., 2001; Coombs et al., 2002; Izbekov et al., 2002). This is because: (1) plagioclase is extremely common in rocks from volcanic arcs; (2) plagioclase crystallizes over a wide range of temperatures and persists as a stable crystallizing phase throughout cooling and eruption; and (3) the compositional and textural zoning patterns develop during primary growth are preserved in plagioclase because the CaAl–NaSi diffusion ex-

change within the crystal structure is relatively slow (Grove et al., 1984).

Lavas erupted from Unzen volcano in SW Japan (Fig. 1) over the past 500,000 years (Hoshizumi et al., 1999) show evidence of magma mingling between at least 2 distinct magmas, basaltic and dacitic, in the form of abundant disequilibrium phenocryst textures and assemblages and evenly distributed basaltic to andesitic enclaves (Browne et al., 2006). Many enclaves contain resorbed plagioclase in a matrix composed predominantly of acicular plagioclase microphenocrysts and glass (Fig. 2). In this study, we report results that focus on the manner in which magma mingling occurs in the Unzen magma chamber as recorded by plagioclase phenocrysts. We combine textural observations with high resolution major and trace element analysis traverses of plagioclase crystals from enclaves and host lavas from Unzen erupted over the past 500,000 years, as well as from an andesitic lava flow erupted in 1663 that lacks enclaves. Textural analyses combined with electron microprobe analysis (EMPA) and laser ablation inductively coupled plasma mass spectrometry (LA ICP-MS) of plagioclase crystals are interpreted to indicate that some crystals that were derived from the host dacite magma are engulfed by a more mafic magma during intrusion events. In response to the change in

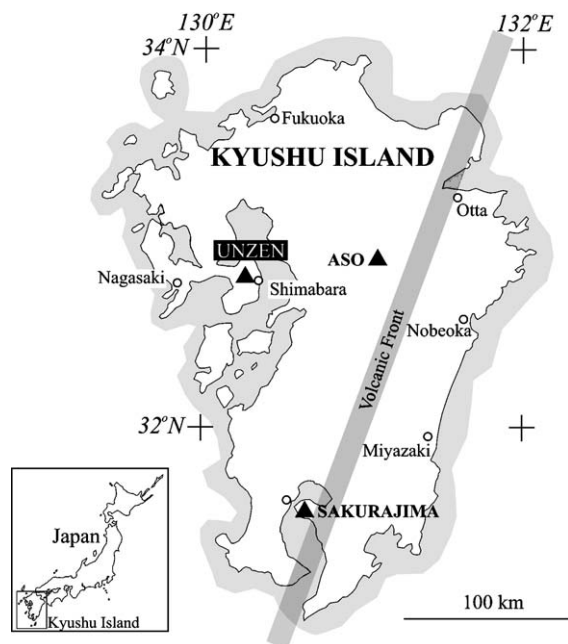


Fig. 1. Location map of Unzen volcano on Kyushu Island, Japan. The location of the Japanese volcanic front (shaded), and other nearby active volcanic centers (solid triangles), including Aso and Sakurajima, are also indicated.

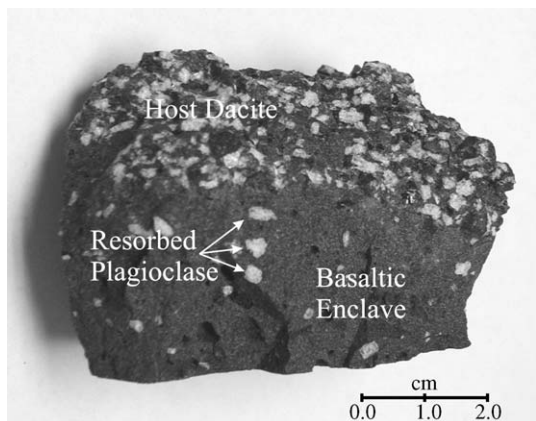


Fig. 2. Photograph of a chilled basaltic enclave and crystal-rich host dacite lava (sample U2A-E). The texture of chilled enclaves is characterized as being glass-rich and porphyritic, with resorbed plagioclase in a fine-grained (20–50  $\mu\text{m}$ ) matrix of acicular crystals. The margins of enclaves are fine-grained, glass-rich, and crenulated, indicative of rapid cooling (e.g. Bacon, 1986). A 2 cm scale is provided.

temperature and composition of the surrounding melt, these crystals become partially resorbed and subsequently overgrown by rims of dramatically different composition. Over time, some of these partially resorbed plagioclase crystals are recycled back into the host dacite magma.

## 2. Geologic framework

Unzen volcano resides in a depression known as the Unzen graben (Hoshizumi et al., 1999), which is located approximately 70 km behind the volcanic front of SW Japan (Fig. 1). The Unzen volcanic edifice is composed of a complex of several different volcanic vents constructed upon many lava domes, lava flows, and pyroclastic and landslide deposits. K–Ar ages of the oldest Unzen deposits range from ~300 to 200 ka (Hoshizumi et al., 1999; Uto et al., 2002), although some deposits yield K–Ar ages of 500 ka (NEDO, 1988). Several different volcanic edifices, including Mayuyama, Fugendake, Myokendake and Nodake represent more recent Unzen deposits (K–Ar,  $^{14}\text{C}$ , and fission track ages from ~100 ka to present) (Uto et al., 2002). The deposits of Unzen volcano are lava domes, thick lava flows, and pyroclastic deposits that contain remarkably repetitive compositions that range from andesite to dacite (~57–67 wt.%  $\text{SiO}_2$ ) (Nakada and Motomura, 1999). Unzen lavas are predominantly characterized by the presence of abundant mafic enclaves (Browne et al., 2006), and a complex mineral assemblage of large

(0.1 to 1 cm) plagioclase and hornblende phenocrysts with minor orthopyroxene, clinopyroxene, quartz, biotite, olivine, magnetite, ilmenite, and apatite.

## 3. Materials and analytical methods

Three sample suites are used in this study. Suite 1 consists of enclave-bearing dacite lava and dacite block and ash flow sequences intersected by the USDP-1 drill hole (752 m depth; Hoshizumi et al., 2002), which was the first drill hole of the Unzen Scientific Drilling Project (<http://hakone.eri.u-tokyo.ac.jp/vrc/usdp/index.html>). These samples range in age from 18,750 yr BP to 500,000 ka (Uto et al., 2002), and were acquired at the USDP core storage facility located at the Geological Survey of Japan in Tsukuba City. The core was described, photographed and archived by the Geological Survey of Japan. Suite 2 consists of enclave-bearing dacite block and ash flow deposits from the 1991–1995 eruption collected in January 2002. Samples of enclave-bearing lavas from suites 1 and 2 are referred to as “host” lavas in this study. Suite 3 is from an enclave-free andesite lava flow erupted from Unzen volcano in the year 1663.

The major element compositions of plagioclase from the host lavas, enclaves and 1663 lava were analyzed by using a Cameca SX-50 Electron Microprobe, equipped with four wavelength-dispersive spectrometers and one energy-dispersive spectrometer, located at the University of Alaska, Fairbanks. For all analyses, an accelerating voltage of 15 keV, a beam current of 10 nA, and a 2–3  $\mu\text{m}$  focused electron beam was used.

Sr and Ba contents in multiple spots along microprobe traverses of representative plagioclase phenocrysts were analyzed by using a Micromass Plasma ICP-MS coupled with a Cetac LSX 200+ laser ablation system at Michigan State University. The 266 nm Nd:YAG laser was focused to a 25  $\mu\text{m}$  sampling spot size and propagated into the sample at a rate of 1  $\mu\text{m}/\text{s}$ . The data acquisition time was 1 min, starting before the ablation and continued after ablation had stopped. The first 0.3 min of data acquisition were used to measure the background. After ~0.3 min of data acquisition, ablation was initiated and continued for 10 s. As the ablated material reached the detector, the signal was observed as a well-developed peak. Results were quantified using the height of the peak above background for each element. Concentrations of Sr and Ba were calculated by using peak intensities of  $^{88}\text{Sr}$ ,  $^{138}\text{Ba}$ , and  $^{44}\text{Ca}$  calibrated against a NIST 612 glass standard and EMPA determinations of Ca in

analyzed spots as outlined in Norman et al. (1996). Precision for Sr and Ba is better than  $\pm 6\%$  and  $\pm 9\%$ , respectively ([http://www.glg.msu.edu/facilities/jb-1aXRF\\_ICP-MS-Stats.XLS](http://www.glg.msu.edu/facilities/jb-1aXRF_ICP-MS-Stats.XLS)).

#### 4. Types of plagioclase

##### 4.1. Host lava samples

Plagioclase is the most abundant phenocryst phase in Unzen host lavas, accounting for 15–25 vol.% of rock samples. Plagioclase found in host lavas fall into two populations based on texture and composition. The most common population (>90%) consists of large grains (0.25–1 cm in length) that are oscillatory-zoned (Table 1, Fig. 3A–B), with core compositions of  $An_{50}$  to  $An_{65}$  and medial zones ranging from  $An_{45}$  to  $An_{70}$  (Table 2, Fig. 4). The second, less common plagioclase population (<10%) consists of grains with a coarsely sieved interior (Table 1, Fig. 3C) with core compositions of  $An_{70}$  to  $An_{80}$ . Coarsely sieved interiors result from the presence of abundant inclusions of pyroxene, hornblende and glass (melt), and contain an extensive network of interconnecting inclusions that pervades the crystals interior.

Resorption zones surround the interiors of 35–45% of oscillatory-zoned host plagioclase phenocrysts (Table 1, Fig. 3B), and 5–15% of coarsely sieved host plagioclase (Fig. 3D). Resorption zones on host plagioclase range widely in thickness from 30 to 400  $\mu\text{m}$ , and are

composed of a profuse network micron-sized glass (melt) inclusions and plagioclase of abruptly higher An composition ( $An_{70}$ – $An_{90}$ ) compared to the interior region of the phenocrysts (Table 2, Fig. 4). The texture and composition of these resorption zones strongly resemble those replicated by Nakamura and Shimakita (1998) in heating experiments.







Clear rims enclose virtually all plagioclase phenocrysts found in the host lavas. Rims are often defined by euhedral to subhedral crystal faces. In grains with resorption zones, rims exhibit strong normal zoning patterns across a total thickness that ranges from 10 to 80  $\mu\text{m}$ . Rim compositions immediately adjacent to resorption zones range from  $An_{75}$  to  $An_{88}$  (referred to as resorption zone rims in tables). The outermost rim of all plagioclase crystals in contact with matrix (referred to as outer rims in tables) ranges in composition from  $An_{50}$  to  $An_{70}$ .

##### 4.2. 1663 lava samples

In the 1663 andesite lava, plagioclase is also the most common phase, accounting for 15–20 vol.%. The majority of plagioclase phenocrysts from the 1663 lava can be divided into the same two populations with the same proportions from host lavas based on texture and composition. The first plagioclase population consists of oscillatory-zoned grains ranging from 0.05 to 0.6 cm in length (Fig. 3E), with core compositions of  $An_{45}$  to  $An_{65}$  and rim compositions of  $An_{50}$  to  $An_{75}$  (Table 3, Fig. 4). Coarsely sieved plagioclase phenocrysts ( $An_{75}$ – $An_{85}$  cores) are less common in the 1663 lava. All plagioclase from these two populations are surrounded by resorption zones, which are characterized by a densely sieved texture of glass inclusions and high An plagioclase ( $An_{75}$ – $An_{85}$ ) (Fig. 3E). Plagioclase resorption zones in the 1663 lava have a narrower range of thickness (30–90  $\mu\text{m}$ ) compared to that of other host lavas (30–400  $\mu\text{m}$ ). A third population of plagioclase exists in the 1663 lava, and is represented by smaller phenocrysts (0.02 to 0.04 cm) with resorption zone cores ranging from  $An_{85}$  to  $An_{95}$  in composition (Fig. 3F).

Clear, euhedral to subhedral rims surrounds all 1663 lava plagioclase phenocrysts where in contact with the melt (glass). Rims are 10 to 30  $\mu\text{m}$  thick, and exhibit strong normal zoning patterns from the rim immediately surrounding resorption zones ( $An_{72}$ – $An_{91}$ ) to the crystal edge ( $An_{70}$ – $An_{85}$ ). Many 1663 plagioclase phenocrysts appear broken as evidenced by their cracked morphology and truncated oscillatory zoning patterns. It is unlikely, however, that these crystals were fractured

Table 1  
Model abundance and illustrations of different plagioclase populations in Unzen host lavas, enclaves, and 1663 lava

|                                       |   | Host lavas | Enclaves   | 1663 lava |
|---------------------------------------|---|------------|------------|-----------|
| Oscillatory-zoned                     |  | <i>M</i>   | A          | A         |
| Oscillatory-zoned with resorption rim |  | <i>m</i>   | <i>m</i>   | <i>M</i>  |
| Coarsely sieved                       |  | <i>m</i>   | <i>m-t</i> | A         |
| Coarsely sieved with resorption rim   |  | <i>t</i>   | A          | <i>t</i>  |
| Resorption core                       |  | <i>m</i>   | <i>m</i>   | <i>m</i>  |
| Microphenocryst                       |  | A          | <i>M</i>   | A         |

Notes: *M* > 20%, 20% > *m* > 1%, *t* < 1%; A = absent.

Table 2  
Representative analyses of host plagioclase phenocrysts

| Sample             | Phenocryst region | SiO <sub>2</sub> | Al <sub>2</sub> O <sub>3</sub> | FeO  | CaO   | Na <sub>2</sub> O | K <sub>2</sub> O | Total  | μm*  | An**  | Sr/Ba |
|--------------------|-------------------|------------------|--------------------------------|------|-------|-------------------|------------------|--------|------|-------|-------|
| 435.20–435.25 H1-2 | Core              | 57.01            | 26.77                          | 0.27 | 8.59  | 5.90              | 0.49             | 99.03  | 0    | 57.34 | 4.16  |
|                    |                   | 56.47            | 27.46                          | 0.22 | 8.99  | 6.07              | 0.39             | 99.59  | 146  | 58.18 | 4.07  |
|                    |                   | 58.03            | 26.14                          | 0.21 | 8.26  | 6.47              | 0.49             | 99.61  | 293  | 54.26 | 4.19  |
|                    |                   | 58.97            | 25.21                          | 0.24 | 8.02  | 6.07              | 0.70             | 99.21  | 457  | 54.25 | 4.63  |
|                    |                   | 58.92            | 26.15                          | 0.17 | 7.77  | 6.49              | 0.54             | 100.04 | 749  | 52.50 | 4.11  |
|                    | Resorption zone   | 48.02            | 31.56                          | 0.81 | 15.97 | 3.06              | 0.19             | 99.61  | 1105 | 83.09 | NA    |
|                    |                   | 47.75            | 30.24                          | 0.57 | 15.52 | 3.52              | 0.50             | 98.10  | 1169 | 79.44 | 25.12 |
|                    |                   | 54.93            | 26.68                          | 0.26 | 10.16 | 5.15              | 0.29             | 97.47  | 1278 | 65.12 | 4.04  |
|                    |                   | 58.00            | 26.36                          | 0.27 | 8.04  | 6.39              | 0.45             | 99.51  | 0    | 54.03 | 4.36  |
|                    |                   | 55.94            | 27.75                          | 0.28 | 9.48  | 5.81              | 0.37             | 99.63  | 102  | 60.54 | 3.96  |
| 435.20–435.25 H1-3 | Core              | 58.75            | 25.95                          | 0.14 | 7.84  | 6.60              | 0.51             | 99.79  | 182  | 52.44 | 4.17  |
|                    |                   | 56.95            | 27.07                          | 0.39 | 8.84  | 6.09              | 0.40             | 99.74  | 253  | 57.66 | 3.98  |
|                    |                   | 57.53            | 26.46                          | 0.34 | 8.15  | 6.60              | 0.47             | 99.55  | 496  | 53.55 | 3.81  |
|                    |                   | 57.15            | 26.61                          | 0.35 | 8.85  | 6.05              | 0.47             | 99.48  | 577  | 57.58 | 4.73  |
|                    |                   | 47.93            | 31.82                          | 0.87 | 15.46 | 2.94              | 0.24             | 99.26  | 1110 | 82.94 | NA    |
|                    | Resorption zone   | 47.17            | 32.04                          | 0.74 | 15.51 | 3.26              | 0.24             | 98.96  | 1188 | 81.59 | 21.52 |
|                    |                   | 56.23            | 30.92                          | 0.54 | 7.58  | 5.41              | 0.16             | 100.84 | 1255 | 57.64 | 5.86  |
|                    |                   | 56.31            | 27.85                          | 0.27 | 9.30  | 5.76              | 0.41             | 99.90  | 0    | 60.12 | 4.83  |
|                    |                   | 57.13            | 27.41                          | 0.16 | 8.64  | 6.13              | 0.43             | 99.90  | 199  | 56.84 | 5.34  |
|                    |                   | 58.06            | 26.29                          | 0.23 | 7.91  | 6.42              | 0.50             | 99.41  | 397  | 53.34 | 5.18  |
| 602.80–602.85 H1-2 | Core              | 58.63            | 26.79                          | 0.29 | 8.38  | 6.33              | 0.51             | 100.93 | 560  | 55.06 | 4.23  |
|                    |                   | 58.91            | 26.32                          | 0.26 | 7.60  | 6.53              | 0.56             | 100.18 | 686  | 51.74 | 4.75  |
|                    |                   | 58.68            | 25.90                          | 0.30 | 7.33  | 6.98              | 0.55             | 99.74  | 812  | 49.33 | 4.09  |
|                    |                   | 58.95            | 25.93                          | 0.18 | 7.38  | 6.63              | 0.55             | 99.62  | 955  | 50.69 | 4.71  |
|                    |                   | 59.03            | 25.99                          | 0.18 | 7.59  | 6.74              | 0.54             | 100.07 | 1010 | 51.04 | 4.73  |
|                    | Outer rim         | 58.63            | 25.59                          | 0.19 | 7.60  | 6.53              | 0.64             | 99.18  | 1028 | 51.46 | 4.78  |
|                    |                   | 55.82            | 27.46                          | 0.17 | 9.40  | 5.79              | 0.37             | 99.01  | 0    | 60.41 | 6.08  |
|                    |                   | 57.04            | 27.10                          | 0.20 | 8.66  | 6.18              | 0.46             | 99.64  | 217  | 56.60 | 5.69  |
|                    |                   | 56.08            | 27.07                          | 0.31 | 9.27  | 5.85              | 0.30             | 98.88  | 236  | 60.12 | 5.69  |
|                    |                   | 56.85            | 26.99                          | 0.31 | 8.84  | 6.11              | 0.36             | 99.46  | 470  | 57.74 | 5.77  |
| U1-A H1-4          | Core              | 55.48            | 27.76                          | 0.27 | 9.22  | 5.83              | 0.32             | 98.88  | 634  | 59.99 | 5.69  |
|                    |                   | 57.11            | 26.58                          | 0.28 | 8.43  | 6.48              | 0.44             | 99.32  | 706  | 54.92 | 8.21  |
|                    |                   | 57.54            | 26.55                          | 0.23 | 8.17  | 6.73              | 0.43             | 99.65  | 724  | 53.29 | 9.69  |
|                    |                   | 48.67            | 32.22                          | 0.37 | 14.92 | 2.82              | 0.10             | 99.10  | 735  | 83.63 | NA    |
|                    |                   | 51.89            | 28.63                          | 0.65 | 14.05 | 3.06              | 0.34             | 98.62  | 1122 | 80.52 | 14.43 |
|                    | Resorption zone   | 57.58            | 26.76                          | 0.24 | 7.97  | 6.65              | 0.51             | 99.71  | 1151 | 52.68 | 5.55  |

Oxide units in weight percent, \*microns measured from phenocryst core, \*\*anorthite content in weight percent.

during ascent or emplacement because the crystal fragments are also surrounded by dusty zones of high An content ranging from An<sub>75</sub> to An<sub>85</sub> and finally enclosed by thin, clear, An<sub>75</sub>–An<sub>85</sub> rims.

#### 4.3. Enclave samples

Plagioclase microphenocrysts are the most common mineral phase in enclaves, accounting for 50–65 vol.% of the enclaves, and are characterized as either acicular or tabular-shaped grains ranging from 60 to 80 μm long and 20 to 40 μm wide (Table 1, Fig. 5). Enclave plagioclase microphenocrysts exhibit strong normal zoning gradients from core to rim, with core compositions ranging between An<sub>80</sub> and An<sub>92</sub>, and rim compositions of An<sub>52</sub>–An<sub>70</sub>.

Plagioclase phenocrysts are commonly found in enclaves, accounting for between 3 and 5 vol.% (Fig. 2). These plagioclase grains range in size from 0.2 to 8 mm in diameter, and commonly have oscillatory-zoned (An<sub>45</sub> to An<sub>70</sub>) cores (Table 4, Fig. 4) that are invariably enclosed by resorption zones composed of a tightly packed network micron-size glass inclusions and An<sub>84</sub> to An<sub>92</sub> plagioclase (Fig. 5). The thicknesses of these resorption zones range from 30 to 500 μm when comparing grains in one enclave to those in another. However, the thicknesses of resorption zones on plagioclase within the same enclave are nearly identical. This observation holds true even when oscillatory-zoned plagioclase occur in clusters of 2–4 overlapping grains. In this case, resorption zones continue across grain boundaries parallel to the contact

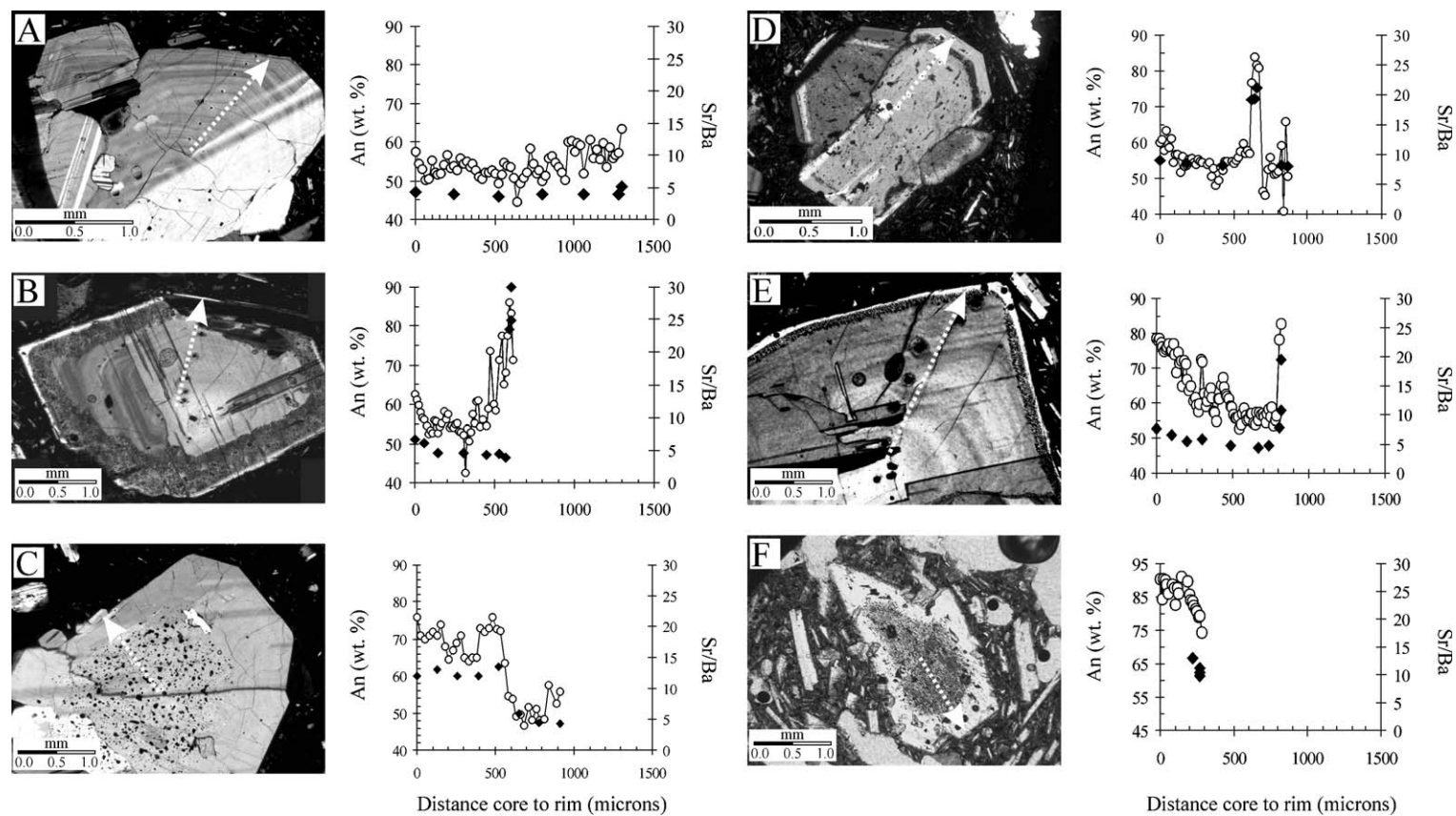


Fig. 3. Photomicrographs of different Unzen plagioclase types from host dacite samples (A, B, C and D) and 1663 lava (E and F) with wt.% An (open symbols) plotted with Sr/Ba ratios (filled symbols) along core to rim sampling transects. A, oscillatory-zoned plagioclase (437.15-H1-4); B, oscillatory-zoned plagioclase with resorption zone (435.20-H1-3); C, coarsely sieved plagioclase without resorption zone (546.45-H1-3); D, coarsely sieved plagioclase with resorption zone (602.80-H1-3); E, oscillatory-zoned plagioclase with resorption zone (1663B04a); and F, resorption zone core plagioclase (1663B07b). Arrows indicate path of sampling transects for electron microprobe analyses. Surface pits represent points of laser ablation ICP-MS analyses. One millimeter scales are provided. Note the strong correlation between fluctuations in An content and Sr/Ba.

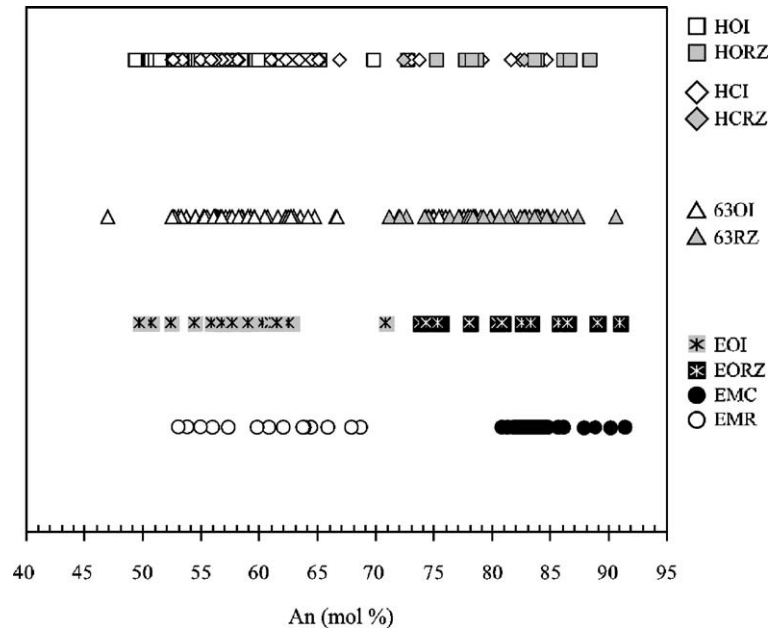


Fig. 4. Compositions of different regions of plagioclase phenocrysts and microphenocrysts in host dacite lavas (HOI-host lava oscillatory interior, HORZ-host lava oscillatory resorption zone rims, HCI-host lava coarsely sieved interior, HCRZ-host lava coarsely sieved resorption zone rim), 1663 andesite lava (63OI-1663 lava oscillatory interior, 63RZ-1663 lava resorption zone rim), and the hybrid basalt enclaves (EMC-enclave microphenocryst core, EMR-enclave microphenocryst rim, EOI-enclave porphyritic oscillatory interior, EORZ-enclave porphyritic resorption zone rim).

between the crystal rim and enclave matrix. A thin, clear rim ( $<30 \mu\text{m}$ ) encloses the resorption zone. Like other Unzen plagioclase grains, these rims are strongly normally zoned, with resorption zone rim compositions ranging from  $\text{An}_{73}$  to  $\text{An}_{92}$  and outer rim compositions ranging from  $\text{An}_{49}$  to  $\text{An}_{67}$  (Table 4, Fig. 5). Finally, phenocrystic plagioclases with coarsely sieved cores ( $\text{An}_{72}$  to  $\text{An}_{85}$ ) rarely exist in enclaves, and typically are not surrounded by resorption zones.

## 5. Plagioclase Sr/Ba ratios

Specific points within plagioclase phenocrysts from Unzen host lavas, enclaves, and the 1663 lava were examined with laser ablation ICP-MS to determine Sr and Ba zoning patterns (Fig. 3 and 5). Ba and Sr were measured along the same transects as those performed using EMPA. Resorption zones were not analyzed via laser ablation ICP-MS because of the interference between the 25- $\mu\text{m}$ -wide spot size and the abundance of micron-sized glass inclusions. However, laser ablation ICP-MS analysis was performed in areas immediately adjacent to resorption zones (RZ Rims) and at the outermost crystal edge (Outer Rim).

Sr and Ba measurements were employed in this study because their abundant trace elements in plagioclase (substituting for Ca) and their partitioning behavior is controlled by changes in crystal structure (Blundy and Wood, 1991; Giletti and Casserly, 1994), which is predominately influenced by changing melt temperature, melt composition, water content, and pressure. In most crystals, fluctuations in the Sr/Ba ratio mirror those in anorthite content (Fig. 6). Oscillatory-zoned cores from host lavas have Sr/Ba ratios ranging from 2.3 to 9.7, which is similar to that determined by Nakai et al. (2002), who found a Sr/Ba ratios range of 3.3–4.8 for host lava plagioclase phenocrysts with non-resorbed rims. The interior regions of coarsely sieved crystals and resorption zone rims from host lava plagioclase have distinctly different Sr/Ba ratios, ranging from 3.9 to 21.2 and 9.2 to 25.1, respectively. Likewise, oscillatory-zoned interiors of plagioclase phenocrysts from the 1663 lava flow contain Sr/Ba ratios ranging from 3.3 to 11.8, to be compared with their resorbed rims, which have Sr/Ba ratios of 4.4 to 20.6. The interiors of large oscillatory-zoned plagioclase phenocrysts found within enclaves have equivalent Sr/Ba ratios as oscillatory-zoned interiors of phenocrysts in host lavas (3.4–10.1) and have resorption zone rims with comparable Sr/Ba

Table 3  
Representative analyses of 1663 lava plagioclase phenocrysts

| Sample              | Phenocryst region   | SiO <sub>2</sub> | Al <sub>2</sub> O <sub>3</sub> | FeO   | CaO   | Na <sub>2</sub> O | K <sub>2</sub> O | Total  | μm*   | An**  | Sr/Ba |
|---------------------|---------------------|------------------|--------------------------------|-------|-------|-------------------|------------------|--------|-------|-------|-------|
| UZN1663A-01         | Core                | 55.47            | 31.29                          | 0.18  | 8.10  | 4.19              | 0.21             | 99.44  | 10    | 64.80 | 5.73  |
|                     |                     | 55.46            | 31.29                          | 0.24  | 8.15  | 4.10              | 0.14             | 99.38  | 20    | 65.78 | 6.06  |
|                     |                     | 54.16            | 30.40                          | 0.17  | 9.27  | 5.91              | 0.37             | 100.28 | 111   | 59.61 | 6.25  |
|                     |                     | 55.32            | 28.30                          | 0.20  | 9.72  | 6.01              | 0.34             | 99.89  | 353   | 60.49 | 4.92  |
|                     | 55.18               | 29.26            | 0.23                           | 8.76  | 6.33  | 0.43              | 100.19           | 696    | 56.44 | 5.21  |       |
|                     | Resorption zone     | 49.82            | 30.46                          | 0.86  | 15.79 | 2.14              | 0.28             | 99.35  | 855   | 86.71 | NA    |
|                     | Resorption zone rim | 49.48            | 32.46                          | 0.55  | 15.26 | 2.88              | 0.08             | 100.71 | 887   | 83.75 | 15.29 |
| Outer rim           | 58.64               | 27.11            | 0.16                           | 8.77  | 6.46  | 0.37              | 101.51           | 921    | 56.22 | 4.44  |       |
| UZN1663A-02         | Core                | 55.40            | 28.72                          | 0.37  | 10.38 | 5.35              | 0.31             | 100.53 | 144   | 64.71 | 11.84 |
|                     |                     | 53.54            | 31.42                          | 0.26  | 10.96 | 3.91              | 0.20             | 100.29 | 156   | 72.73 | 8.65  |
|                     |                     | 57.44            | 26.93                          | 0.19  | 8.76  | 6.38              | 0.43             | 100.13 | 735   | 56.26 | 4.54  |
|                     |                     | 56.67            | 28.23                          | 0.27  | 9.64  | 5.96              | 0.27             | 101.04 | 903   | 60.74 | 4.27  |
|                     | 56.23               | 28.05            | 0.13                           | 10.21 | 5.70  | 0.32              | 100.64           | 1361   | 62.91 | 4.84  |       |
|                     | 57.95               | 27.14            | 0.09                           | 8.79  | 6.44  | 0.42              | 100.83           | 1614   | 56.17 | 4.13  |       |
|                     | Resorption zone     | 49.18            | 30.44                          | 0.88  | 15.73 | 2.91              | 0.24             | 99.38  | 1726  | 83.32 | NA    |
| Resorption zone rim | 49.26               | 32.53            | 0.54                           | 15.12 | 2.76  | 0.13              | 100.34           | 1797   | 83.95 | 16.94 |       |
| Outer rim           | 57.35               | 27.23            | 0.25                           | 9.39  | 6.21  | 0.42              | 100.85           | 1834   | 58.61 | 4.31  |       |
| UZN1663B-04a        | Core                | 51.21            | 31.42                          | 0.38  | 12.23 | 3.75              | 0.16             | 99.15  | 0     | 75.77 | 7.58  |
|                     |                     | 52.45            | 30.77                          | 0.18  | 11.11 | 4.16              | 0.20             | 98.87  | 101   | 71.82 | 7.87  |
|                     |                     | 55.43            | 29.34                          | 0.17  | 10.19 | 5.34              | 0.25             | 100.72 | 202   | 64.58 | 5.48  |
|                     |                     | 53.09            | 30.30                          | 0.10  | 11.27 | 4.59              | 0.20             | 99.55  | 303   | 70.17 | 5.78  |
|                     | 55.58               | 27.41            | 0.15                           | 9.41  | 6.11  | 0.38              | 99.04            | 486    | 59.18 | 4.69  |       |
|                     | 57.15               | 27.23            | 0.23                           | 8.62  | 6.61  | 0.40              | 100.24           | 667    | 55.15 | 4.41  |       |
|                     | Resorption zone     | 50.02            | 30.85                          | 0.92  | 15.46 | 2.76              | 0.28             | 100.29 | 884   | 83.57 | NA    |
| Resorption zone rim | 50.08               | 31.61            | 0.68                           | 15.13 | 2.81  | 0.11              | 100.42           | 917    | 83.82 | 13.00 |       |
| Outer rim           | 55.43               | 26.99            | 0.22                           | 9.14  | 6.16  | 0.40              | 98.34            | 938    | 58.22 | 4.73  |       |
| UZN1663B-05         | Core                | 54.70            | 30.73                          | 0.18  | 10.76 | 4.24              | 0.17             | 100.78 | 0     | 70.93 | 3.90  |
|                     |                     | 58.16            | 26.46                          | 0.20  | 8.77  | 6.42              | 0.43             | 100.44 | 141   | 56.15 | 4.18  |
|                     |                     | 54.52            | 28.86                          | 0.19  | 9.72  | 5.49              | 0.34             | 99.12  | 241   | 62.51 | 4.33  |
|                     |                     | 55.66            | 28.20                          | 0.22  | 10.05 | 5.68              | 0.31             | 100.12 | 342   | 62.66 | 5.11  |
|                     | 52.32               | 30.47            | 0.64                           | 13.10 | 3.97  | 0.30              | 100.80           | 443    | 75.42 | 4.60  |       |
|                     | Resorption zone     | 49.86            | 31.48                          | 0.87  | 14.87 | 3.02              | 0.22             | 100.32 | 638   | 82.11 | NA    |
|                     | Resorption zone rim | 50.61            | 31.23                          | 0.62  | 14.27 | 3.29              | 0.16             | 100.18 | 664   | 80.53 | 10.09 |
| Outer rim           | 49.72               | 31.97            | 0.65                           | 15.50 | 3.07  | 0.13              | 101.04           | 694    | 82.89 | 7.74  |       |

Oxide units in weight percent, \*microns measured from phenocryst core, \*\*anorthite content in weight percent.

ratios to those in host lavas (10.1–26.2). Cores of enclave plagioclase microphenocrysts contain Sr/Ba ratios of 3.4 to 13.3, with rims characterized by Sr/Ba ratios of 1.7 to 5.8.

## 6. Discussion

The Sr/Ba ratio of Unzen plagioclase phenocrysts and microphenocrysts strongly increases with An content (Fig. 6). This is consistent with the results of Blundy and Wood (1991), who found that the partitioning of Sr and Ba between plagioclase and melt is primarily dependent on the structure of a plagioclase crystal, where Ba is less compatible than Sr as An content increases. The change in Sr/Ba ratios with plagioclase composition from samples analyzed in our study is also broadly consistent with the predicted changes in Sr and Ba crystal-melt partitioning as a

function of changing plagioclase composition (Fig. 6, dashed line) (e.g. Blundy and Wood, 1991). Strong correlations also exist between plagioclase texture and composition with respect to major element and Sr/Ba ratios, where the oscillatory-zoned regions of host lava plagioclase interiors are compositionally and texturally identical to the interior regions of plagioclase from the 1663 lava flow and the interior regions of enclave plagioclase phenocrysts. Similarly, resorption zone rims on host lava plagioclase have a compositional range that matches that of resorption rims on plagioclase from the 1663 lava flow and enclaves, as well as that of enclave microphenocryst cores.

In host lavas, oscillatory-zoned plagioclase (An<sub>45</sub> to An<sub>70</sub>) is the most common phase, indicating that it most likely crystallized from the host dacite. This inference is supported by plagioclase compositions from phase equilibria experiments on the dacite host magma that



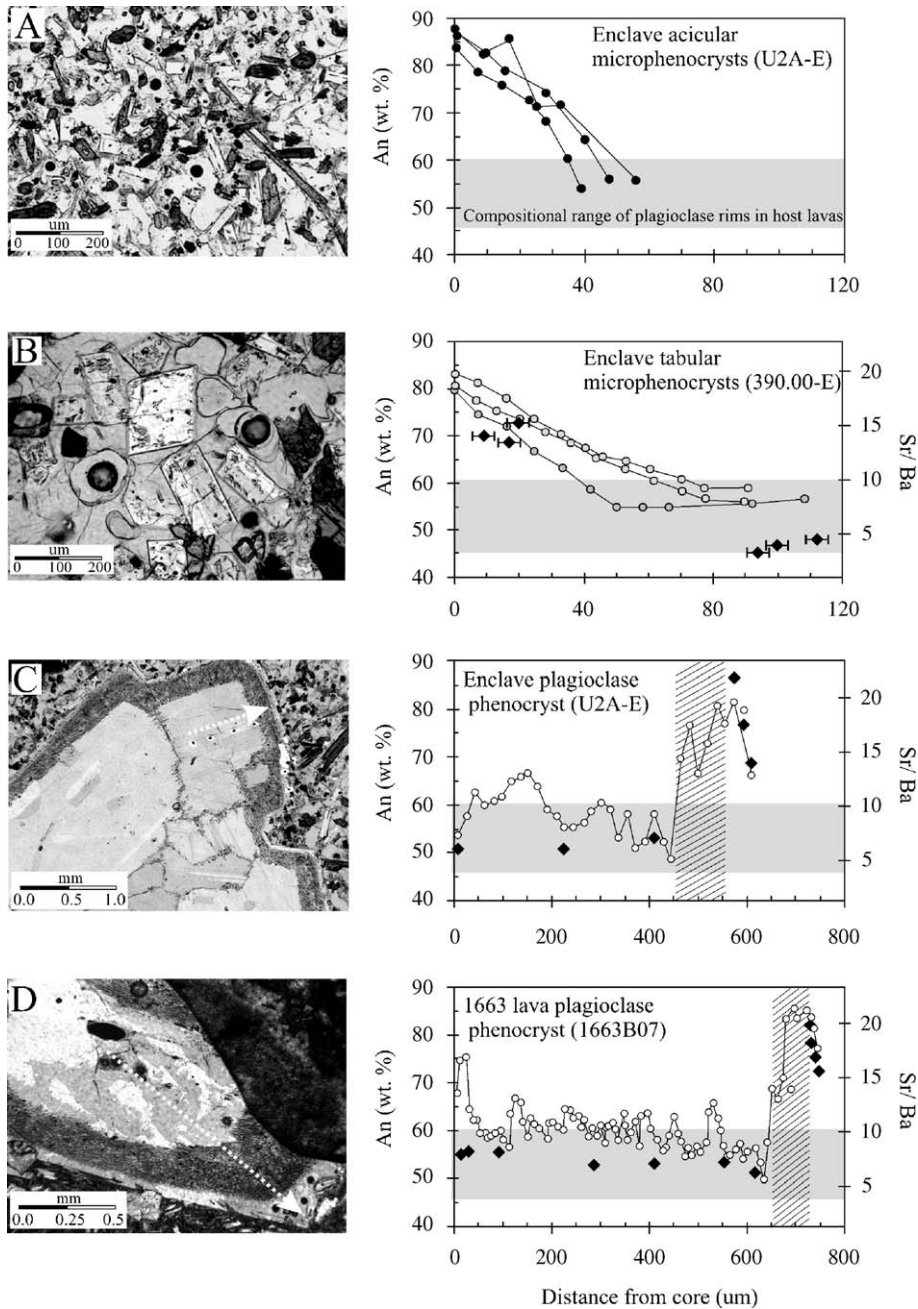


Fig. 5. Photomicrographs of different Unzen plagioclase types from basaltic enclaves and 1663 lava with wt.% An (open symbols) plotted with Sr/Ba ratios (filled symbols) along core to rim sampling transects. A, Acicular microphenocrysts (U2A-E); B, tabular microphenocrysts (390.00-E); C, aggregate of oscillatory-zoned plagioclase phenocrysts surrounded by resorption zone (U2A-E); and oscillatory-zoned plagioclase phenocryst with resorption zone from 1663 lava (1663B07). Arrows indicate path of sampling transects for electron microprobe analyses. Shaded regions on graphs indicate range of plagioclase compositions from host lava, hatched regions indicate resorption zone. One millimeter scale bar provided. Surface pits represent points of laser ablation ICP-MS analyses.

erupted from Unzen in 1991 (Venezky and Rutherford, 1999). Coarsely sieved plagioclase phenocrysts also exist in host dacite lavas and the 1663 lava, but are interpreted to have originated from the intruding basaltic

magma because the coarsely sieved plagioclase cores are similar in An content and Sr/Ba ratio to enclave plagioclase microphenocrysts. The texture of coarsely sieved plagioclases is similar to coarsely sieved

Table 4

Representative analyses of plagioclase (M, microphenocryst; MA, acicular microphenocryst; P, phenocryst) from enclaves

| Sample                  | Phenocryst region | SiO <sub>2</sub> | Al <sub>2</sub> O <sub>3</sub> | FeO  | CaO   | Na <sub>2</sub> O | K <sub>2</sub> O | Total  | um*  | An**  | Sr/Ba |
|-------------------------|-------------------|------------------|--------------------------------|------|-------|-------------------|------------------|--------|------|-------|-------|
| 153.85–153.90 E1-1 (M)  | Core              | 56.35            | 27.62                          | 0.25 | 9.50  | 5.69              | 0.43             | 99.84  | 10   | 60.82 | 8.40  |
|                         | Outer rim         | 55.12            | 28.31                          | 0.31 | 10.42 | 5.39              | 0.36             | 99.91  | 60   | 64.44 | 5.56  |
| 153.85–153.90 E2-1 (M)  | Core              | 55.62            | 27.64                          | 0.33 | 9.91  | 5.72              | 0.35             | 99.57  | 16   | 62.02 | 12.75 |
|                         | Outer rim         | 53.58            | 28.92                          | 0.46 | 11.40 | 4.87              | 0.33             | 99.56  | 108  | 68.67 | 5.65  |
| 153.85–153.90 E2-2 (M)  | Core              | 57.62            | 27.12                          | 0.25 | 8.69  | 6.37              | 0.47             | 100.52 | 16   | 55.96 | 7.28  |
|                         | Outer rim         | 52.87            | 30.19                          | 0.25 | 12.50 | 4.38              | 0.23             | 100.42 | 50   | 73.06 | 4.81  |
| 153.85–153.90 E2-4 (M)  | Core              | 53.92            | 28.52                          | 0.28 | 10.81 | 5.36              | 0.24             | 99.13  | 17   | 65.87 | 13.30 |
|                         | Outer rim         | 57.46            | 26.89                          | 0.26 | 9.06  | 6.31              | 0.44             | 100.42 | 62   | 57.31 | 5.83  |
| 546.40–546.45 E1-1 (MA) | Core              | 48.98            | 31.30                          | 0.87 | 15.95 | 2.61              | 0.12             | 99.83  | 0    | 85.39 | NA    |
|                         |                   | 49.87            | 30.08                          | 1.25 | 15.89 | 2.67              | 0.21             | 99.97  | 8    | 84.66 | NA    |
|                         |                   | 49.02            | 32.65                          | 0.53 | 15.24 | 2.84              | 0.09             | 100.37 | 18   | 83.87 | NA    |
|                         |                   | 49.05            | 32.42                          | 0.45 | 15.01 | 2.68              | 0.12             | 99.73  | 26   | 84.28 | NA    |
|                         |                   | 49.26            | 31.93                          | 0.57 | 14.72 | 3.00              | 0.15             | 99.63  | 35   | 82.37 | NA    |
|                         |                   | 50.31            | 31.99                          | 0.44 | 14.50 | 3.39              | 0.14             | 100.77 | 44   | 80.42 | NA    |
|                         |                   | 52.86            | 31.85                          | 0.57 | 11.56 | 3.28              | 0.23             | 100.35 | 53   | 76.71 | NA    |
|                         |                   | 53.18            | 29.67                          | 0.58 | 11.66 | 4.81              | 0.44             | 100.34 | 62   | 68.95 | NA    |
|                         |                   | 54.49            | 28.87                          | 0.26 | 12.05 | 4.86              | 0.44             | 100.97 | 70   | 69.45 | NA    |
|                         |                   | 54.89            | 27.49                          | 0.37 | 9.65  | 5.85              | 0.53             | 98.78  | 0    | 60.20 | 5.08  |
| 602.80–602.85 E1-1 (P)  | Core              | 56.11            | 27.58                          | 0.35 | 9.26  | 6.09              | 0.32             | 99.71  | 431  | 59.09 | 4.78  |
|                         |                   | 55.81            | 27.62                          | 0.25 | 9.21  | 6.01              | 0.39             | 99.29  | 575  | 59.00 | 4.32  |
|                         |                   | 56.72            | 26.66                          | 0.09 | 8.85  | 6.32              | 0.43             | 99.07  | 647  | 56.73 | 4.82  |
|                         |                   | 57.63            | 25.98                          | 0.23 | 8.11  | 6.80              | 0.59             | 99.34  | 790  | 52.32 | 4.96  |
|                         |                   | 57.32            | 25.67                          | 0.40 | 9.37  | 5.29              | 0.64             | 98.69  | 1365 | 61.24 | 9.16  |
|                         |                   | 50.86            | 29.84                          | 1.14 | 14.86 | 3.16              | 0.24             | 100.10 | 1405 | 81.38 | NA    |
|                         |                   | 53.96            | 28.56                          | 0.94 | 12.30 | 3.92              | 0.46             | 100.14 | 1510 | 73.74 | 12.37 |
|                         |                   | 56.45            | 26.93                          | 0.27 | 9.85  | 5.18              | 0.66             | 99.34  | 1538 | 62.78 | 8.15  |
|                         |                   | 56.29            | 26.79                          | 0.32 | 8.82  | 6.28              | 0.32             | 98.82  | 0    | 57.20 | 6.33  |
|                         |                   | 55.79            | 26.50                          | 0.24 | 8.95  | 6.13              | 0.38             | 97.99  | 273  | 57.89 | 5.37  |
| U2-A E1-2 (P)           | Core              | 56.92            | 26.37                          | 0.11 | 8.54  | 6.15              | 0.41             | 98.50  | 546  | 56.56 | 4.87  |
|                         |                   | 58.05            | 25.66                          | 0.21 | 7.58  | 6.88              | 0.50             | 98.88  | 800  | 50.67 | 5.91  |
|                         |                   | 56.86            | 26.04                          | 0.25 | 8.42  | 6.20              | 0.43             | 98.20  | 946  | 55.95 | 8.43  |
|                         |                   | 55.92            | 27.02                          | 0.18 | 9.31  | 6.12              | 0.37             | 98.92  | 1055 | 58.92 | 5.60  |
|                         |                   | 49.82            | 30.21                          | 1.05 | 15.53 | 3.18              | 0.24             | 100.03 | 1096 | 81.95 | NA    |
|                         |                   | 48.23            | 31.26                          | 0.99 | 14.46 | 2.96              | 0.11             | 98.01  | 1174 | 82.49 | 19.86 |
|                         |                   | 60.70            | 24.12                          | 0.49 | 7.19  | 6.02              | 1.28             | 99.80  | 1208 | 49.62 | 3.42  |

Oxide units in weight percent, \*microns measured from phenocryst core, \*\*anorthite content in weight percent.

textures experimentally replicated by rapid decompression from high pressure (Nelson and Montana, 1992), which may be the expected path for a mafic magma prior to intrusion (Vance, 1965; Stormer, 1972; Nelson and Montana, 1992; Johannes et al., 1994).

Plagioclase microphenocrysts with calcic cores (An<sub>80</sub> to An<sub>92</sub>) are the dominant phase in the Unzen enclaves, consistent with the interpretation that plagioclase microphenocrysts originate from the enclave-forming basaltic magma. The interiors of large plagioclase phenocrysts in enclaves, however, are oscillatory-zoned and identical in both major element and Sr/Ba ratio to the interiors of plagioclase grains in the host lavas, suggesting that they originate from the host dacite magma, and not from the enclave forming basaltic magma. This suggests that the intruding basalt

engulfs host-derived phenocrysts during replenishment events.

Resorption zones surround every oscillatory-zoned plagioclase phenocrysts found in enclaves. The An content and resorption zone texture described in this study strongly resemble experimentally developed plagioclase grains that formed in response to sudden heating events (Tsuchiyama and Takahashi, 1983; Tsuchiyama, 1985; Nakamura and Shimakita, 1998). In addition, the compositions of resorption zones are characterized as having equivalently high An content and Sr/Ba ratios compared with microphenocryst cores, which is also consistent with crystallization at higher temperatures (Blundy and Wood, 1991). This suggests that the texture and composition of resorption zones surrounding the oscillatory-zoned interiors of enclave phenocrystic plagioclase record the mineralogical

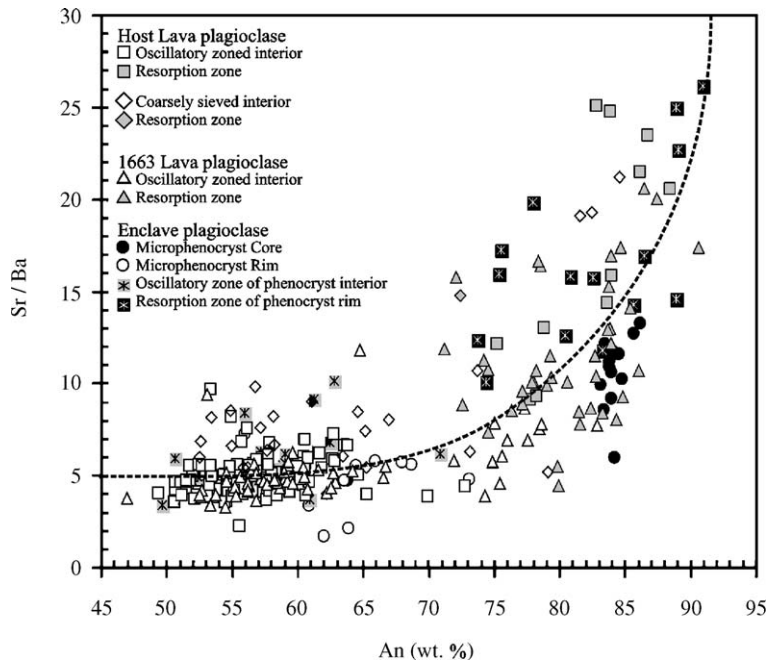


Fig. 6. Sr/Ba ratios of Unzen plagioclase plotted against An content (wt.%) for host dacite lavas (HOI-host lava oscillatory interior, HORZ-host lava oscillatory resorption zone rims, HCI-host lava coarsely sieved interior, HCRZ-host lava coarsely sieved resorption zone rim), 1663 andesite lava (63OI-1663 lava oscillatory interior, 63RZ-1663 lava resorption zone rim), and the basalt enclaves (EMC-enclave microphenocryst core, EMR-enclave microphenocryst rim, EOI-enclave porphyritic oscillatory interior, EORZ-enclave porphyritic resorption zone rim). Note the strong correlation between Sr/Ba ratio and increasing An content, which occurs as a result of Ba becoming less compatible than Sr with increasing An content due to changes in the plagioclase crystal structure (Blundy and Wood, 1991). Also note that broad correlation between the samples analyzed in our study and what is predicted by Blundy and Wood's (1991) empirically derived relationship for changing partition coefficients of Sr and Ba as a function of An weight fraction.

response to being engulfed by intruding magma during basaltic replenishment events.

The thickness of resorption zones can be used to estimate the amount of time required for engulfment of host phenocrysts by intruding basaltic magma. Resorption zones on oscillatory-zoned interiors of enclave plagioclase phenocrysts range in thickness from 30 to 500  $\mu\text{m}$ . This range in thickness requires 0.3 to 8 days to develop given a surrounding temperature range of between 950 and 1050  $^{\circ}\text{C}$  according to experiments (Tsuchiyama and Takahashi, 1983; Tsuchiyama, 1985; Nakamura and Shimakita, 1998), which is consistent with the geothermometry of the enclave-forming basalt (955–1040  $^{\circ}\text{C}$ , Venezky and Rutherford, 1999; Browne et al., 2006). However, simple conduction model predicts that a 30-cm diameter enclave at 1000  $^{\circ}\text{C}$  would approach thermal equilibration with the surrounding host magma (800  $^{\circ}\text{C}$ ) in an hour (e.g. Jaeger, 1968), thus requiring that intruding basalt does not mix with host magma while in the form of blobs or enclaves because rapid cooling leaves insufficient time for the resorption zones to form. Therefore, resorption zones likely develop on host-derived plagioclases while they

are incorporated into the intruding basalt magma, and continue to form as the intruded magma is dispersed.

The presence of resorption zones on oscillatory-zoned plagioclase and coarsely sieved plagioclase in host dacite lavas, which are texturally and compositionally identical to those observed in plagioclase phenocrysts contained in enclaves, requires that plagioclases that were once engulfed by intruding basaltic magma be recycled back into the host magma over time. This could occur through the disaggregation of enclaves, which is consistent with the presence of deteriorating enclaves in Unzen samples (Browne et al., 2006). Similar interpretations have been made based on textural, compositional, and isotopic evidence (Clynne, 1989, 1999; Tepley et al., 1999; Tepley et al., 2000) from other volcanoes (e.g. Lassen Peak 1915, USA; Chaos Craggs, USA; El Chichón, Mexico).

Following the formation of resorption zones on engulfed plagioclase grains, their crystallization is recorded by the presence of clear rims that enclose the densely sieved resorption zones. The combined width of resorption zones and rims may be used as criteria for estimating the duration that phenocrysts reside in the

host dacite magma chamber in the time between their encounter with a basaltic intrusion and eruption. Plagioclase rims that enclose resorption zones on grains found in the host dacite lavas are euhedral and range widely from 10 to 80  $\mu\text{m}$  in width. In contrast, rims that enclose resorption zones in plagioclase grains from the 1663 lava flow and the enclaves have a narrower range in thickness from 10 to 30  $\mu\text{m}$ . Using plagioclase crystallization rates that have been calibrated experimentally ( $1.0\text{--}1.6 \times 10^{-9}$  cm/s, e.g. Hammer and Rutherford, 2002), host lava plagioclase rims require between 10 and 92 days compared to only 10 to 30 days in the case of the 1663 andesite lava in addition to the time required for resorption zone development (10–38 and 10–100 days, respectively). Of course, these timescales do not account for differences in melt composition or temperature between the host lava (dacite) and 1663 lava (andesite) magmas, which will strongly influence crystallization rates, and are therefore considered to be approximations. The wide range in thicknesses of host lava plagioclase rims can be interpreted in two ways, though subject to the previously mentioned uncertainties. First, it may reflect the casual progression of enclave disaggregation over time, where some engulfed plagioclase are recycled to the host soon after intrusion compared with others that remain suspended in enclaves for longer amounts of time. Second, the wide range in host lava plagioclase rim thickness may reflect several discrete replenishment events in between eruptions.

Most host-derived plagioclase phenocrysts are clearly not engulfed by intruding basaltic magma during a replenishment event, as evidenced by the abundance of oscillatory-zoned plagioclase phenocrysts in host dacite lavas that are not enclosed by resorption zones. The presence of both resorbed and non-resorbed plagioclase phenocrysts is ubiquitous in Unzen dacitic lavas. This is consistent with replenishment events resulting in mingling of only a portion of the magma body that is eventually erupted (e.g. Koyaguchi and Kaneko, 1999). The 1663 lava flow appears to be the rare exception to this rule because all 1663 lava plagioclase phenocrysts contain a resorption zone of comparable thickness, similar to that observed in enclaves. Resorption zones on the 1663 plagioclase are also identical in texture and composition to those observed in enclave plagioclases and those found in host lavas. The 1663 lava therefore appears to demonstrate that all of the erupted magma was the product of complete and thorough mixing between intruded basalt and host dacite. In this situation, such thorough mixing is only expected to result from a replenishment scenario where the mass fraction of

intruded basalt accounted for the majority of the mixture ( $\geq 50\%$ ) (Kouchi and Sunagawa, 1985; Bacon, 1986; Sparks and Marshall, 1986). In addition, the similarity of the 1663 lava plagioclase population to that observed in the enclaves is consistent with the idea that the two differ only in post-replenishment history. Whereas the 1663 lava may represent a magma that was erupted after thorough mixing with the intruding basaltic magma, the enclave-bearing dacite host lavas resulted from interaction with lesser amounts of intruded basalt and went through the additional step of quenching and dispersal of enclaves. This interpretation is supported by the fact that the 1663 andesitic lava flow does not contain enclaves.

## 7. Conclusions

Trace element analysis via laser ablation ICP-MS combined with EMP analyses and textural characterization provide a useful means of identifying unique plagioclase phenocryst populations in magmas of different origins where magma mixing has played a dominant role in their petrogenesis. In this case, we integrated micrometer-scale analyses on distinct plagioclase textures, such as oscillatory zoning bands or resorption zones, which record phenocryst exchange events between intruded basaltic magma and host dacite magma. This finding demonstrates that magma mixing is a principal mechanism for the origin of the textural and mineralogical diversity that is diagnostic of Unzen magmas.

Intrusions of basaltic magma into the Unzen dacite magma chamber have occurred throughout the history of the volcano. When a basaltic intrusion event occurs, many host-derived plagioclase phenocrysts are engulfed by the basaltic magma. Engulfed plagioclase phenocrysts develop a resorption zone in response to the dramatically different surrounding melt temperature and composition, and crystallize a rim composition identical in An content and Sr/Ba ratio to plagioclase microphenocrysts inherent to the intruding basalt. Over time, the engulfed plagioclase grains are recycled back into the host magma as enclaves disaggregate (e.g. Clyne, 1989; Tepley et al., 1999). This produces a diverse population of phenocrysts with distinctly different crystallization histories from distinctly different magmas. A unique case of unusually thorough mixing between intruded basalt and host dacite at Unzen appears to be recorded by the enclave-free 1663 andesite lava. In this case, all of the host-derived plagioclase phenocrysts were engulfed by the intruding basalt and erupted together, consistent with the mass fraction of the basalt accounting for the

majority of the mixture ( $\geq 50\%$ ) (Kouchi and Sunagawa, 1985; Bacon, 1986; Sparks and Marshall, 1986). Using experimentally determined crystallization rates, we approximate that plagioclase phenocrysts appear to exist in the Unzen chamber between 0.5 and 3 months from the time of their encounter with a basaltic intrusion until eruption.

## Acknowledgments

This project is one of the many outcomes from the Unzen Scientific Drilling Project (<http://hakone.eri.u-tokyo.ac.jp/vrc/usdp/index.html>), which continues to be cooperatively managed and supported at all stages by Kozo Uto and Hideo Hoshizumi of the Geologic Survey of Japan (GSJ), and the Ministry of Education, Culture, Sports, Science, and Technology (MEXT). We remain deeply appreciative to be involved in such an interesting project and are very grateful for the opportunity to have been granted access to the USDP cores, which are property of the GSJ. We thank Setsuya Nakada for providing us with a sample of the 1663 lava. We also thank the following people for their helpful suggestions and thought-provoking discussions: George Bergantz, Carrie Browne, Jonathon Dehn, Cynthia Gardner, James Gardner, Nobuo Geshi, Pavel Izbekov, Jessica Larsen, John Pallister, Jennifer Reynolds, and Robert Wiebe. Ken Severin assisted with electron microscopy, especially with respect to ensuring that the electron microprobe located at the University of Alaska Fairbanks Advanced Instrumentation Laboratory functioned properly. In addition, we are especially grateful to Arata Kurihara and Akikazu Matsumoto for their assistance and dedication during sampling at the USDP drill core storage facility in Tsukuba City. We also sincerely appreciate Dougal Jerram, Frank Tepley, and Michael Clyne for their review of this paper. Finally, we express thanks to the National Science Foundation for their cooperation and patience, in addition to their financial support of this research (Grant EAR-0310406 to JCE and Grant EAR-0309773 to TAV and LCP).

## References

- Anderson, A.T., 1983. Oscillatory zoning of plagioclase: Nomarski interference contrast microscopy of etched Polish sections. *Am. Mineral.* 68, 125–129.
- Bacon, C.R., 1986. Magmatic inclusions in silicic and intermediate volcanic rocks. *J. Geophys. Res.* 91, 6091–6112.
- Bindeman, I.N., Bailey, J.C., 1999. Trace elements in anorthite megacrysts from the Kurile Arc: a window to across-arc geochemical variations in magma compositions. *Earth Planet. Sci. Lett.* 169, 209–226.
- Blundy, J.D., Wood, B.J., 1991. Crystal-chemical controls on the partitioning of Sr and Ba between plagioclase feldspar, silicate melts, and hydrothermal solutions. *Geochem. Cosmochim. Acta* 55, 193–209.
- Browne, B.L., Eichelberger, J.C., Patino, L.C., Vogel, T.A., Uto, K., Hoshizumi, H., Dehn, J., 2006. The generation of porphyritic and equigranular enclaves during magma recharge events at Unzen volcano. *Japan. J. Petrol.* 47, 301–328.
- Clyne, M.A., 1989. The disaggregation of quenched magmatic inclusions contributes to chemical diversity in silicic lavas of Lassen Peak, California. *Bull. New Mexico Bureau of Mines and Mineral Resources*, vol. 131, p. 54.
- Clyne, M.A., 1999. A complex magma mixing origin for rocks erupted in 1915, Lassen Peak, California. *J. Petrol.* 40, 105–132.
- Coombs, M.C., Eichelberger, J.C., Rutherford, M.J., 2002. Experimental and textural constraints on mafic enclave formation in volcanic rocks. *J. Volcanol. Geotherm. Res.* 119, 125–144.
- Davidson, J.P., Tepley III, F.J., 1997. Recharge in volcanic systems: evidence from isotopic profiles of phenocrysts. *Science* 275, 826–829.
- Davidson, J.P., Tepley, F.J. III, Knesel K.M., 1998. Isotopic fingerprinting may provide insights into evolution of magmatic systems. *EOS Transactions, Amer. Geophys. Union*, 79: 185, 189, 193.
- Davidson, J.P., Tepley III, F.J., Palacz, Z., Meffan Main, S., 2001. Magma recharge, contamination and residence times revealed by in situ laser ablation isotopic analysis of feldspar in volcanic rocks. *Earth Planet. Sci. Lett.* 184, 427–442.
- Druitt, T.H., Bacon, C.R., 1989. Petrology of the zoned calcalkaline magma chamber of Mount Mazama, Crater Lake, Oregon. *Contrib. Mineral. Petrol.* 101, 245–259.
- Dunbar, N.W., Cashman, K.V., Dupré, R., 1994. Crystallization processes of anorthoclase phenocrysts in the Mount Erebus magmatic system: evidence from crystal composition, crystal size distributions, and volatile contents of melt inclusions. *Antarct. Res. Ser.* 66, 129–146.
- Feeley, T.C., Dungan, M.A., 1996. Compositional and dynamic controls on mafic–silicic magma interactions at continental arc volcanoes; evidence from Cordón El Guadal, Tatara—San Pedro Complex, Chile. *J. Petrol.* 37, 1547–1577.
- Gamble, J.A., Wood, C.P., Price, R.C., Smith, I.E.M., Stewart, R.B., Waight, T., 1999. A fifty year perspective of magmatic evolution on Ruapehu Volcano, New Zealand: verification of open system behaviour in an arc volcano. *Earth Planet. Sci. Lett.* 170, 301–314.
- Geist, D.J., Myers, J.D., Frost, C.D., 1988. Megacryst-bulk rock isotopic disequilibrium as an indicator of contamination process: the Edgecumbe Volcanic Field, SE Alaska. *Contrib. Mineral. Petrol.* 99, 105–112.
- Giletti, B.J., Casserly, J.E.D., 1994. Strontium diffusion kinetics in plagioclase feldspars. *Geochim. Cosmochim. Acta* 58, 3785–3793.
- Grove, T.L., Baker, M.B., Kinzler, R.J., 1984. Coupled CaAl–NaSi diffusion in plagioclase feldspar: Experiments and applications to cooling rate speedometry. *Geochem. Cosmochim. Acta* 48, 2113–2121.
- Hammer, J.E., Rutherford, M.J., 2002. An experimental study of the kinetics of decompression-induced crystallization in silicic melts. *J. Geophys. Res.* 107, 8–24.
- Heiken, G., Eichelberger, J.C., 1980. Eruptions at Chaos Crags, Lassen Volcanic National Park, California. *J. Volcanol. Geotherm. Res.* 7, 443–481.

- Hoshizumi, H., Uto, K., Watanabe, K., 1999. Geology and eruptive history of Unzen Volcano, Shimabara Peninsula, Kyushu, SW Japan. *J. Volcanol. Geotherm. Res.* 89, 81–94.
- Hoshizumi, H., Uto, K., Matsumoto, A., Xu, S., Oguri, K., 2002. Geology of Unzen volcano and core stratigraphy of the flank drilling (abstract). Unzen Workshop 2002: International Workshop on the Unzen Scientific Drilling Project, pp. 4–8.
- Izbekov, P.E., Eichelberger, J.C., Patino, L.C., Vogel, B.V., Ivanov, B. V., 2002. Calcic cores of plagioclase phenocrysts in andesite from Karymsky volcano: evidence for rapid introduction by basalt replenishment. *Geology* 30, 799–802.
- Jaeger, J.C., 1968. Cooling and solidification of igneous rocks. In: Hess, H.H., Poldervaart, A. (Eds.), *Basalts*, volume 2. John Wiley and Sons, Inc., New York, New York, pp. 503–536.
- Johannes, W., Koepke, J., Behrens, H., 1994. Partial melting reactions of plagioclases and plagioclase-bearing systems. In: Parsons, I.E. (Ed.), *Feldspars and the Reactions*. D. Reidel Publishing Company, Edinburgh, United Kingdom, pp. 161–194.
- Knesel, K.M., Davidson, J.P., Duffield, W.A., 1999. Evolution of silicic magma through assimilation and subsequent recharge: evidence from Sr isotopes in sanidine phenocrysts, Taylor Creek Rhyolite, NM. *J. Petrol.* 40, 773–786.
- Kouchi, A., Sunagawa, I., 1985. A model for mixing basaltic and dacitic magmas as deduced from experimental data. *Contrib. Mineral. Petrol.* 89, 17–23.
- Koyaguchi, T., Kaneko, K., 1999. A two-stage thermal evolution model of magmas in continental crust. *J. Petrol.* 40, 241–254.
- Lofgren, G.E., 1980. Experimental studies on the dynamic crystallization of silicate melts. In: Hargraves, R.B. (Ed.), *Physics of Magmatic Processes*. Princeton University Press, Princeton, NJ, pp. 487–551.
- Nakada, S., Motomura, Y., 1999. Petrology of the 1991–1995 eruption at Unzen; effusion pulsation and groundmass crystallization. *J. Volcanol. Geotherm. Res.* 89, 173–196.
- Nakada, S., Bacon, C.R., Gartner, A.E., 1994. Origin of phenocrysts and compositional diversity in per-Mazama rhyodacite lavas, Crater Lake, Oregon. *J. Petrol.* 35, 127–162.
- Nakai, S., Maeda, Y., Nakada, S., 2002. Common origin of plagioclase in the last three eruptions of Unzen volcano, Japan (abstract). Unzen Workshop 2002: International Workshop on the Unzen Scientific Drilling Project, pp. 58–59.
- Nakamura, M., Shimakita, S., 1998. Dissolution origin and syntaxation compositional change of melt inclusion in plagioclase. *Earth Planet. Sci. Lett.* 161, 119–133.
- NEDO (New Energy Development Organization), 1988. *Western District of Unzen. Report on the Promotion and Development of Geothermal Energy*, vol. 15, p. 1060 (in Japanese).
- Nelson, S.T., Montana, A., 1992. Sieve-textured plagioclase in volcanic rocks produced by rapid decompression. *Am. Mineral.* 77, 1242–1249.
- Norman, M.D., Pearson, N.J., Sharma, A., Griffin, W.L., 1996. Quantitative analysis of trace elements in geological materials by laser ablation ICP-MS: instrumental operating conditions and calibration values of NIST glasses. *Geostand. Newsl.* 20, 776–798.
- Pallister, J.S., Hoblitt, R.P., Meeker, G.P., Knight, R.J., Siems, D.F., 1996. Magma mixing at Mount Pinatubo; petrographic and chemical evidence from the 1991 deposits. In: Newhall, C.G., Punongbayan, R.S. (Eds.), *Fire and Mud; Eruptions and Lahars of Mount Pinatubo, Philippines*. University of Washington Press, Seattle, WA, pp. 687–731.
- Pearce, T.H., Griffin, M.P., Kolisnik, A.M., 1987. Magmatic crystal stratigraphy and constraints on magma chamber dynamics: laser interference results on individual phenocrysts. *J. Geophys. Res.* 92, 13745–13752.
- Singer, B.S., Dungan, M.A., Layne, G.D., 1995. Textures and Sr, Ba, Mg, Fe, K, and Ti compositional profiles in volcanic plagioclase: Clues to the dynamics of calc-alkaline magma chambers. *Am. Mineral.* 80, 776–798.
- Sparks, R.S.J., Marshall, L.A., 1986. Thermal and mechanical constraints on mixing between mafic and silicic magmas. *J. Volcanol. Geotherm. Res.* 29, 99–124.
- Stimac, J.A., Pearce, T.H., 1992. Textural evidence of mafic–felsic magma interaction in dacite lavas, Clear Lake, California. *Am. Mineral.* 77, 795–809.
- Stimac, J.A., Pearce, T.H., Donnelly Nolan, J.M., Hearn Jr., B.C., 1990. The origin and implications of undercooled andesitic inclusions in rhyolites, Clear Lake Volcanics, California. *J. Geophys. Res.* 95, 17729–17746.
- Stormer, J.C., 1972. Mineralogy and petrology of the Raton–Clayton volcanic field, northeastern New Mexico. *Geol. Soc. Amer. Bull.* 83, 3299–3322.
- Tepley III, F.J., Davidson, J.P., Clyne, M.A., 1999. Magmatic interactions as recorded in plagioclase phenocrysts of Chaos Crags, Lassen Volcanic Center, California. *J. Petrol.* 40, 787–806.
- Tepley III, F.J., Davidson, J.P., Tilling, R.I., Arth, J.G., 2000. Magma mixing, recharge and eruption histories in plagioclase phenocrysts from El Chichón Volcano, Mexico. *J. Petrol.* 41, 1397–1411.
- Tsuchiyama, A., 1985. Dissolution kinetics of plagioclase in the melt of the system: diopside–albite–anorthite, and origin of dusty plagioclase in andesites. *Contrib. Mineral. Petrol.* 89, 1–16.
- Tsuchiyama, A., Takahashi, E., 1983. Melting kinetics of a plagioclase feldspar. *Contrib. Mineral. Petrol.* 84, 345–354.
- Uto, K., Nakada, S., Hoshizumi, H., Shimizu, H., 2002. Overview of the Unzen Scientific Drilling Project and the progress of its first phase [abstract: V10/01P/A01-001]. International Union of Geodesy and Geophysics 2003 Meeting, Sapporo, Japan.
- Vance, J.A., 1965. Zoning in igneous plagioclase: patchy zoning. *J. Geol.* 73, 636–651.
- Venezky, D.Y., Rutherford, M.J., 1999. Petrology and Fe–Ti oxide reequilibration of the 1991 Mount Unzen mixed magma. *J. Volcanol. Geotherm. Res.* 89, 213–230.
- Zellmer, G.F., Blake, S., Vance, D., Hawkesworth, C., Turner, S., 1999. Plagioclase residence times at two island arc volcanoes (Kameni Islands, Satorini, and Soufriere, St. Vincent) determined by Sr diffusion systematics. *Contrib. Mineral. Petrol.* 136, 345–357.